Geophys. J. Int. (1993) **115,** 251–263

Scattering of elastic waves by a spherical inclusion—II. Limitations of asymptotic solutions

Valeri A. Korneev and Lane R. Johnson

Department of Geology and Geophysics, and Center for Computational Seismology, Lawrence Berkeley Laboratory, University of California, Berkeley, California 94720, USA

Accepted 1993 March 8. Received 1993 March 1; in original form 1992 May 20

SUMMARY

Starting with the exact solution for the scattering of a plane *P* wave by a homogeneous spherical inclusion, various types of approximate solutions are developed and discussed. The standard Rayleigh and Mie approximations are extended to the case of inclusions having arbitrary contrasts in material properties. For the low-contrast case, solutions are developed which are valid over a wide frequency range. Several aspects of these solutions are discussed, including the importance of near-field terms and the relative strength of the scattered *P* and *S* fields. The various types of approximate solutions are compared with each other and with the exact solution by calculating and displaying their normalized scattering cross-sections.

Key words: diffraction, elastic waves, scattering, sphere.

1 INTRODUCTION

Scattering of seismic waves plays a significant role in seismic wave propagation in the earth. Such phenomena as coda-wave excitation, attenuation, precursors, and irregular arrival times are often assumed to be caused by scattering from inhomogeneities in the crust and upper mantle of the earth. The scattering mechanism also plays a role in some of the algorithms for migration and diffraction tomography which are used in exploration seismology.

Exact solutions for scattering problems are known for only a few types of obstacles, and even for these cases the calculations are not easily implemented because of their complicated mathematical representations. The basic approach to the scattering problem which has been developed in such disciplines as optics, acoustics and quantum mechanics makes extensive use of asymptotic solutions to explain the main physical features of the scattered fields. In these disciplines, where the critical parameters of the scattering obstacle and the observation system are usually well known and controllable, experiments can be arranged so that the conditions for the asymptotic solutions are strongly satisfied, and thus these solutions give a satisfactory representation of the observational results. However, in the case of scattered seismic waves the situation is more complicated. Generally there are a wide variety of shapes, locations, boundaries and material properties in the local heterogeneity of the earth's crust and upper mantle which represent the scattering obstacles for the seismic problem. Additional complications arise from the fact that these local heterogeneities are measured with respect to a surrounding material which is itself typically inhomogeneous, but on a larger distance scale. In most cases the parameters of the scattering obstacles are either unknown or poorly known. Furthermore, parameters of the observation system, such as the locations of the sources and receivers and the wavelengths of the incident waves, are typically difficult to control. Therefore, a common situation in seismic problems is that it is unknown whether the conditions necessary for the application of asymptotic solutions are actually satisfied.

Establishing proper conditions for the use of different asymptotic approaches in the treatment of scattered seismic waves is not a simple problem because of a number of reasons:

(1) the broad range in the type and size of scattering obstacles which have to be considered makes it difficult to find an asymptotic approach which is applicable over the entire range.

(2) The fact that several different parameters are involved, some of which are poorly known, makes it difficult to ascertain whether an asymptotic solution is appropriate or not.

(3) It is often necessary to apply a combination of asymptotic solutions and some of these may be incompatible. For

example, for the far field ($r \to \infty$) solution in the case of the Rayleigh approximation ($\omega \to 0$) there is the possibility of a contradiction, because the parameter $kr = \omega r/velocity$ is assumed to be large.

(4) The absence of a set of canonical problems for which exact solutions are known makes it impossible to check the asymptotic solutions by comparing them with the exact solutions.

In the present paper we consider various asymptotic representations of the scattered fields formed when a plane P wave is incident on an elastic spherical inclusion. An exact solution for this problem and methods of calculating it were developed in a previous paper (Korneev & Johnson 1993). This exact solution can be used as the starting point for some of the asymptotic solutions. It can also be compared with the asymptotic solutions as a means of investigating their validity.

2 SOLUTIONS FOR SMALL INCLUSIONS

We begin with a brief review of some of the approximate scattering solutions that are commonly used in seismology. Consider an elastic medium with an inclusion at the centre of joint Cartesian $\{x, y, z\}$ and spherical $\{r, \theta, \phi\}$ coordinate systems. The parameters within the inclusion, denoted by the index ($\nu = 1$), are allowed to be functions of the coordinates

$$\lambda_1 = \lambda_1(x, y, z), \qquad \mu_1 = \mu_1(x, y, z), \qquad \rho_1 = \rho_1(x, y, z). \tag{1}$$

The volume of the inclusion will be denoted by V. The surrounding media, denoted by the index $\nu = 2$ and described by the constant parameters

$$\lambda_2 \equiv \lambda = \text{constant}, \qquad \mu_2 \equiv \mu = \text{constant}, \qquad \rho_2 = \rho = \text{constant} \tag{2}$$

is assumed to be homogeneous. In the equations that follow, material constants without indexes refer to the surrounding media ($\nu = 2$).

Most of the approximate solutions used in seismology involve the Born approximation, which is assumed to be valid in the case of weak single scattering (Aki & Chouet 1975; Sato 1984; Wu & Aki 1985a, 1985b). The actual conditions under which the Born approximation is valid are rather complicated and involve both the dimensions of the inclusion and the contrast in its material properties (Hudson & Heritage 1981), but it is commonly assumed in seismology that they are equivalent to the condition of a small contrast in material properties. By this we mean that the perturbations of the elastic parameters within the inclusion are small in comparison with those in the surrounding medium

$$\frac{|\delta\lambda|}{\lambda} = \frac{|\lambda_1 - \lambda_2|}{\lambda_2} \ll 1, \qquad \frac{|\delta\mu|}{\mu} = \frac{|\mu_1 - \mu_2|}{\mu_2} \ll 1, \qquad \frac{|\delta\rho|}{\rho} = \frac{|\rho_1 - \rho_2|}{\rho_2} \ll 1. \tag{3}$$

Throughout this paper we will be considering an incident plane P wave of the form

$$\tilde{\mathbf{U}}_0 = e^{i\omega[(t - z/V_P)]}\hat{\mathbf{z}} = \mathbf{U}_0 e^{i\omega t}. \tag{4}$$

The wave is travelling along the z axis in the positive direction. The solution to the scattering problem, which includes both the incident and scattered fields, will be written as

$$\tilde{\mathbf{U}} = \mathbf{U}e^{i\omega t} = (\mathbf{U}_0 + \mathbf{U}_p + \mathbf{U}_s)e^{i\omega t} \tag{5}$$

where $\mathbf{U}_p$ and $\mathbf{U}_s$ represent the scattered P and S waves, respectively.

Our next approximation is to consider the solution at low frequencies. Then only the first members of the frequency power series are retained and the solution is

$$\mathbf{U}_p = A\left\{-\frac{\delta\lambda}{\lambda + 2\mu} + \frac{\delta\rho}{\rho}\cos\theta - \frac{2\delta\mu}{\lambda + 2\mu}\cos^2\theta\right\}\hat{\mathbf{r}} \tag{6a}$$

$$\mathbf{U}_s = B\left\{-\frac{\delta\rho}{\rho}\sin\theta + \gamma\frac{\delta\mu}{\mu}\sin 2\theta\right\}\hat{\boldsymbol{\theta}} \tag{6b}$$

and where the following definitions have been used

$$A = k_p^2 \frac{V}{4\pi}\frac{e^{-ik_p r}}{r}, \qquad B = k_s^2 \frac{V}{4\pi}\frac{e^{-ik_s r}}{r}, \qquad k_p = \frac{\omega}{V_p}, \qquad k_s = \frac{\omega}{V_s} \tag{7}$$

$$V_p^{(\nu)} = \sqrt{\frac{\lambda_\nu + 2\mu_\nu}{\rho_\nu}} = d_\nu^{-i}, \qquad V_s^{(\nu)} = \sqrt{\frac{\mu_\nu}{\rho_\nu}}, \qquad \gamma = \frac{V_s}{V_p}. \tag{8}$$

The above result has used only the first term in a power series of frequency and is thus dependent upon the assumption that

$$k_p\bar{R} = \frac{\omega\bar{R}}{V_p} \ll 1 \tag{9}$$

where $\bar{R}$ is the average radius of the inclusion. This is generally known as the Rayleigh–Born approximation. The solution of eq. (6) obviously does not depend upon the shape of the inclusion, but only upon its volume. Thus, for the case of Rayleigh scattering, all parts of a homogeneous inclusion contribute in proportion to their volume and the scattered field is a simple sum of these contributions.

When the wavelength of the incident wave is comparable to the size of the inclusion and (9) is no longer valid, then a different approximation must be used. In Mie scattering the phase differences of the incident wave for different parts of inclusion are taken into account (Chernov 1960). The solution is

$$\mathbf{U}_p = A\int_V\left[-\frac{\delta\lambda(\xi)}{\lambda+2\mu}-\frac{\delta\rho(\xi)}{\rho}\cos\theta-\frac{2\delta\mu(\xi)}{\lambda+2\mu}\cos^2\theta\right]e^{-i\omega S_1\cdot\xi}\,dV(\xi)\hat{\mathbf{r}} \tag{10a}$$

$$\mathbf{U}_s = B\int_V\left[-\frac{\delta\rho(\xi)}{\rho}\sin\theta+\gamma\frac{\delta\mu(\xi)}{\mu}\sin 2\theta\right]e^{-i\omega S_2\xi}\,dV(\xi)\hat{\boldsymbol{\theta}} \tag{10b}$$

where

$$\mathbf{S}_1 = V_p^{-1}\hat{\mathbf{z}} - V_p^{-1}\hat{\mathbf{r}} \qquad \mathbf{S}_2 = V_p^{-1}\hat{\mathbf{z}} - V_s^{-1}\hat{\mathbf{r}}$$

$$S_1 = |\mathbf{S}_1| = 2V_p^{-1}\sin\frac{\theta}{2} \qquad S_2 = |\mathbf{S}_2| = \sqrt{V_p^{-2}+V_s^{-2}-2V_p^{-1}V_s^{-1}\cos\theta}.$$

This approximation is equivalent to assuming that the inclusion is composed of numerous small non-interacting parts, each of which causes a scattered field of the form of eq. (6).

For the case where the scattering volume is a homogeneous sphere of radius R, the expressions in eq. (10) can be integrated to give

$$\mathbf{U}_p = A\left\{-\frac{\delta\lambda}{\lambda+2\mu}+\frac{\delta\rho}{\rho}\cos\theta-\frac{2\delta\mu}{\lambda+2\mu}\cos^2\theta\right\}\frac{j_1(q_1)}{q_1}\mathbf{f} \tag{11a}$$

$$\mathbf{U}_s = B\left\{-\frac{\delta\rho}{\rho}\sin\theta+\gamma\frac{\sigma\mu}{\mu}\sin 2\theta\right\}\frac{j_1(q_2)}{q_2}\hat{\boldsymbol{\theta}} \tag{11b}$$

where

$q_1 = \omega S_1 R$ and $q_2 = \omega S_2 R$

and $j_l(q)$ is the spherical Bessel function of order l.

The solutions of eqs (6) and (10) have been used in many publications for estimating seismic attenuation, explaining the generation of coda waves, obtaining high-frequency asymptotics, and formulating seismic diffraction tomography. In most of these applications, however, valid bounds on the relevant parameters are not established, and possible errors due to the use of asymptotic solutions are not considered. As a result, large errors in the estimated seismic parameters may occur, or invalid solutions may be produced. In a later section we will illustrate these possibilities by comparing the approximate solutions of eqs (6) and (10) with the exact solution for a homogeneous elastic sphere.

3 EXACT SOLUTION FOR THE SPHERE

A method of calculating the exact scattering solution for a homogeneous elastic sphere was presented in detail in a previous paper (Korneev & Johnson 1993), so the results will only be summarized here. The solution for the medium outside of the sphere for the case of an incident plane P wave has the form

$$\mathbf{U} = \mathbf{U}_0 + \mathbf{U}_2 \tag{12}$$

where

$$\begin{aligned}\mathbf{U}_2 = \mathbf{U}_p + \mathbf{U}_s &= \sum_{l\geq 0}\{[a_l h_{l+1}(k_p r) + l b_l h_{l+1}(k_s r)]\mathbf{Y}^+_{l0} \\ &\quad + [-a_l h_{l-1}(k_p r) + (l+1) b_l h_{l-1}(k_s r)]\mathbf{Y}^-_{l0}\}e^{-i[\pi/2(l+1)]} \\ &= \sum_{l\geq 0} e^{-i[\pi/2(l+1)]}(2l+1)\left\{a_l\left[\left((l+1)\frac{h_l(k_p r)}{k_p r} - h_{l-1}(k_p r)\right)P_l(\cos\theta)\hat{\mathbf{r}} - \frac{h_l(k_p r)}{k_p r}\frac{\partial P_l(\cos\theta)}{\partial\theta}\hat{\boldsymbol{\theta}}\right]\right. \\ &\quad \left. + b_l\left[l(l+1)\frac{h_l(k_s r)}{k_s r}P_l(\cos\theta)\hat{\mathbf{r}} + \left(h_{l-1}(k_s r) - \frac{h_l(k_s r)}{k_s r}\right)\frac{\partial P_l(\cos\theta)}{\partial\theta}\hat{\boldsymbol{\theta}}\right]\right\}.\end{aligned} \tag{13}$$

Here $h_k(x)$ are spherical Hankel functions of the second kind. Analytical expressions for the coefficients a_l and b_l are given in Appendix B of Korneev & Johnson (1993), as well as information about the spherical vector system

$$\begin{aligned}\mathbf{Y}^0_{lm} &\equiv \mathbf{Y}^0_{lm}(\theta,\phi) = \mathbf{r}\times\nabla Y_{lm}(\theta,\phi) \\ \mathbf{Y}^+_{lm} &\equiv \mathbf{Y}^+_{lm}(\theta,\phi) = (l+1)\hat{\mathbf{r}}Y_{lm}(\theta,\phi) - r\nabla Y_{lm}(\theta,\phi) \\ \mathbf{Y}^-_{lm} &\equiv \mathbf{Y}^-_{lm}(\theta,\phi) = l\hat{\mathbf{r}}Y_{lm}(\theta,\phi) + r\nabla Y_{lm}(\theta,\phi).\end{aligned} \tag{14}$$

The definitions for the spherical harmonic functions are the usual ones

$$Y_{lm}(\theta, \phi) = e^{im\phi} P_l^m(\cos\theta), \qquad l \geq 0, \quad (-l \leq m \leq l).$$

Any cylindrically symmetric scattered field (as we have for the case of an incident plane P wave) can be represented in the form of eq. (13), where the coefficients a_l correspond to the compressional field and the coefficients b_l correspond to the shear field.

For the purpose of comparing different solutions, we will use the normalized scattering cross-section σ_N, which is the ratio of the flow of the total energy carried outward by the scattered waves to the rate of flow in the incident wave through a normal area equal to the cross-sectional area of the object (geometric shadow of the object). In our case this is

$$\sigma_N = \mathcal{I}m \int_{r=r_0} \frac{(\mathbf{U}_2 \cdot t_r^*(\mathbf{U}_2])\, ds}{\omega\alpha_2(\lambda_2 + 2\mu_2)\pi R^2} = \sigma_N^{(p)} + \sigma_N^{(s)}$$

$$= 4 \sum_{l \geq 0}^{\infty} (2l+1) \left\{ \left| \frac{a_l}{k_p R} \right|^2 + l(l+1)\gamma_2 \left| \frac{b_l}{k_s R} \right|^2 \right\} \tag{15}$$

where $\mathbf{t}_r[\mathbf{U}_2]$ is the stress vector of the field U_2 on the spherical surface of radius r_0, $(r_0 > R)$. The two parts of the scattering cross-section, $\sigma_N^{(p)}$ and $\sigma_N^{(s)}$, represent the P and S fields, respectively. It can be shown that the normalized scattered cross-section σ_N is simply related to the forward-scattered wave in the far field $(r \to \infty)$

$$\mathbf{U}_2(r, 0) \approx \frac{e^{-ik_p r}}{r} A_0 \hat{\mathbf{r}} = i \frac{e^{-ik_p r}}{k_p r} \sum_{l \geq 0}^{\infty} (2l+1) a_l \hat{\mathbf{r}}$$

through the formula

$$\sigma_N = -4 \frac{\mathcal{I}m\{A_0\}}{k_p R^2}. \tag{16}$$

This is the elastodynamic equivalent of an optical theorem.

4 LOW-FREQUENCY SOLUTION FOR AN ELASTIC SPHERE OF ARBITRARY CONTRAST

Starting with the exact solution described in the previous section, it is possible to develop approximate solutions which are more general than the standard approximations given in Section 2. First consider a low-frequency approximation but with no restrictions upon the contrast in material properties. In this case we retain from the solution in eq. (13) only the coefficients that are of lowest degree in frequency, which is ω^3 and appears only in the first three $(l = 0, 1, 2)$ coefficients

$$\begin{aligned} a_0 &= i \frac{\xi^3}{6} \frac{\frac{3}{2}(\lambda_1 - \lambda_2) + \mu_1 - \mu_2}{\frac{1}{2}(\frac{3}{2}\lambda_1 + \mu_1) + \mu_2} \\ a_1 &= -i \frac{\xi^3}{9} \left(\frac{\rho_1}{\rho_2} - 1\right), \qquad b_1 = i \frac{\eta^3}{9} \left(\frac{\rho_2}{\rho_2} - 1\right) \\ a_2 &= i\xi^3 \frac{4}{45} \left(\frac{\mu_2}{\mu_2} - 1\right) \frac{\gamma^2}{D}, \qquad b_2 = -i\eta^3 \frac{2}{45} \left(\frac{\mu_1}{\mu_2} - 1\right) \frac{\gamma}{D} \end{aligned} \tag{17}$$

where

$$\xi = k_p R, \qquad \eta = k_s R$$

$$\gamma = \frac{V_{s2}}{V_{p2}} \equiv \frac{V_s}{V_p}, \qquad D = 1 + \frac{2}{15} \left(\frac{\mu_1}{\mu_2} - 1\right)(3 + 2\gamma^2). \tag{18}$$

Then the solution has the form

$$\begin{aligned} \mathbf{U}_p &= (\mathbf{U}_p)_r \hat{\mathbf{r}} + (\mathbf{U}_p)_\theta \hat{\boldsymbol{\theta}} \\ &= A \left\{ \left[-\frac{1}{2} \frac{\frac{3}{2}(\lambda_1 - \lambda_2) + \mu_1 - \mu_2}{\frac{1}{2}(\frac{3}{2}\lambda_1 + \mu_1) + \mu_2} W_{0r}^p(Z_p) + \left(\frac{\rho_1}{\rho_2} - 1\right) W_{1r}^p(Z_p) \cos\theta + \frac{2}{3} \left(\frac{\mu_1}{\mu_2} - 1\right) \frac{\gamma^2}{D} W_{2r}^p(Z_p)(1 - 3\cos^2\theta) \right] \hat{\mathbf{r}} \right. \\ &\quad \left. - \left[\left(\frac{\rho_1}{\rho_2} - 1\right) W_{1\theta}^p(Z_p) \sin\theta + 2\left(\frac{\mu_1}{\mu_2} - 1\right) \frac{\gamma^2}{D} W_{2\theta}^p(Z_p) \sin 2\theta \right] \hat{\boldsymbol{\theta}} \right\}. \end{aligned} \tag{19a}$$

$$\begin{aligned} \mathbf{U}_s &= (\mathbf{U}_s)_r \hat{\mathbf{r}} + (\mathbf{U}_s)_\theta \hat{\boldsymbol{\theta}} \\ &= B \left\{ \left[2\left(\frac{\rho_1}{\rho_2} - 1\right) W_{1r}^s(Z_s) \cos\theta + 2\left(\frac{\mu_1}{\mu_2} - 1\right) \frac{\gamma}{D} W_{2r}^s(Z_s)(3\cos^2\theta - 1) \right] \hat{\mathbf{r}} \right. \\ &\quad \left. + \left[-\left(\frac{\rho_1}{\rho_2} - 1\right) W_{1\theta}^s(Z_s) \sin\theta + \left(\frac{\mu_1}{\mu_2} - 1\right) \frac{\gamma}{D} W_{2\theta}^s(Z_s) \sin 2\theta \right] \hat{\boldsymbol{\theta}} \right\} \end{aligned} \tag{19b}$$

where the following functions have been introduced.

$$W_{0r}^{p}(Z_p) = 1 - \frac{i}{Z_p}$$

$$W_{1r}^{p}(Z_p) = 1 - 2\frac{1+iZ_p}{Z_p^2}, \qquad W_{2r}^{p}(Z_p) = 1 + \frac{9i - 4iZ_p^2 - 9Z_p}{Z_p^3}$$

$$W_{1\theta}^{s}(Z_s) = 1 - \frac{1+iZ_s}{Z_s^2}, \qquad W_{2\theta}^{s}(Z_s) = 1 + 3\frac{2i - iZ_s^2 - 2Z_s}{Z_s^3}$$

$$W_{1\theta}^{p}(Z_p) = \frac{1+iZ_p}{Z_p^2}, \qquad W_{2\theta}^{p}(Z_p) = \frac{3i - iZ_p^2 - 3Z_p}{Z_p^3}$$

$$W_{1r}^{s}(Z_s) = \frac{1+iZ_s}{Z_s^2}, \qquad W_{2r}^{s}(Z_s) = \frac{3i - iZ_s^2 - 3Z_s}{Z_s^3}. \tag{20}$$

These W functions depend upon frequency ω and radius r of the observation point through the parameters

$$Z_p = k_p r = \frac{\omega r}{V_{p2}}, \qquad Z_s = k_s r = \frac{\omega r}{V_{s2}}.$$

The expression in eq. (19) is a complete low-frequency solution in that it contains both the near-field and far-field parts. All of the distance dependence in the solution is contained in the W functions of eq. (20). We obtain the far-field asymptotic form of the solution if the functions in eq. (20) satisfy the following conditions

$$|W_{0r}^{p}(Z_p)| \approx 1, \quad |W_{1r}^{p}(Z_p)| \approx 1, \quad |W_{2r}^{p}(Z_p)| \approx 1, \quad |W_{1\theta}^{s}(Z_s)| \approx 1, \quad |W_{2\theta}^{s}(Z_s)| \approx 1 \tag{21a}$$

$$|W_{1\theta}^{p}(Z_p)| \approx 0, \quad |W_{2\theta}^{p}(Z_p)| \approx 0, \quad |W_{1r}^{s}(Z_s)| \approx 0, \quad |W_{2r}^{s}(Z_s)| \approx 0. \tag{21b}$$

The functions in eq. (20) are graphed in Fig. 1 for the case of $\gamma = V_s/V_p = Z_p/Z_s = 1/\sqrt{3}$. This figure shows that for $k_p r < 1$ the far-field approximation is definitely not satisfied. As ω increases the situation improves and for $k_p r > 3$ eq. (21a) is satisfied to within 10 per cent. However, the terms of eq. (21b) converge to their asymptotic values much more slowly and, while three of these terms have converged to within 10 per cent of zero for $k_p r > 10$, the $W_{2\theta}^{p}$ term does not decrease to this level until $k_p r > 20$. What this means is that at observation distances r that are only a few times greater than the wavelength, the amplitudes of the scattered waves may be consistent with the far-field approximation but their polarizations will be considerably more complicated than simple P and S waves.

The situation is slightly more complicated than indicated in Fig. 1. In that figure the absolute values of the W functions are plotted, but in eq. (19) it is clear that these functions can combine either constructively or destructively, depending upon the difference in material properties and the azimuth of the observation point. Furthermore, at small distances and low frequencies it can be misleading to consider the individual terms of the solution, as what appears to be a large individual term may be cancelled out by another and not show up in the total solution. Thus in Fig. 2 the effect of the near-field terms in the scattered field is illustrated by showing the complete solutions in the time domain. Here the P wave scattered from a homogeneous spherical inclusion is shown at one azimuth and a distance that is 6 times the radius of the inclusion, which corresponds to $k_p r = 1.2$. The near-field terms make a significant contribution at this distance, affecting both the amplitude and the polarization of the scattered wave.

In the near field zone, where $Z_p \ll 1.0$, $Z_s \ll 1.0$, the P and S components of the scattered field (19) interfere with each other and must be combined to form

$$\mathbf{U} = \frac{V}{4\pi r^3}\left\{\left[\frac{i}{2}\frac{\frac{3}{2}(\lambda_1 - \lambda_2) + \mu_1 - \mu_2}{\frac{1}{2}(\frac{3}{2}\lambda_1 + \mu_1) + \mu_2} Z_p + \left(\frac{\rho_1}{\rho_2} - 1\right)\cos\theta Z_s^2 + i\left(1 - \frac{\gamma^2}{3}\right)\left(\frac{\mu_1}{\mu_2} - 1\right)\frac{Z_p}{D}(3\cos^2\theta - 1)\right]\hat{\mathbf{r}}\right.$$
$$\left. - \left[\frac{(1+\gamma^2)}{2}\left(\frac{\rho_1}{\rho_2} - 1\right)\sin\theta Z_s^2 + i\gamma^2\left(\frac{\mu_1}{\mu_2} - 1\right)\frac{Z_p}{D}\sin 2\theta\right]\hat{\boldsymbol{\theta}}\right\}.$$

Note that the density terms involve Z_s^2, which is small compared to the Z_p in the other terms. Therefore, in the near field the contrast in the elastic moduli produces the major contribution to the scattering.

In the true far field where all of the conditions of eq. (21) are satisfied, the scattered field has the form

$$\mathbf{U}_p = A\left\{-\frac{1}{2}\frac{\frac{3}{2}(\lambda_1 - \lambda_2) + \mu_1 - \mu_2}{\frac{1}{2}(\frac{3}{2}\lambda_1 + \mu_1) + \mu_2} + \left(\frac{\rho_1}{\rho_2} - 1\right)\cos\theta + \frac{2}{3}\left(\frac{\mu_1}{\mu_2} - 1\right)\frac{\gamma^2}{D}(1 - 3\cos^2\theta)\right\}\hat{\mathbf{r}} \tag{22a}$$

$$\mathbf{U}_s = B\left\{-\left(\frac{\rho_1}{\rho_2} - 1\right)\sin\theta + \left(\frac{\mu_1}{\mu_2} - 1\right)\frac{\gamma}{D}\sin 2\theta\right\}\hat{\boldsymbol{\theta}}. \tag{22b}$$

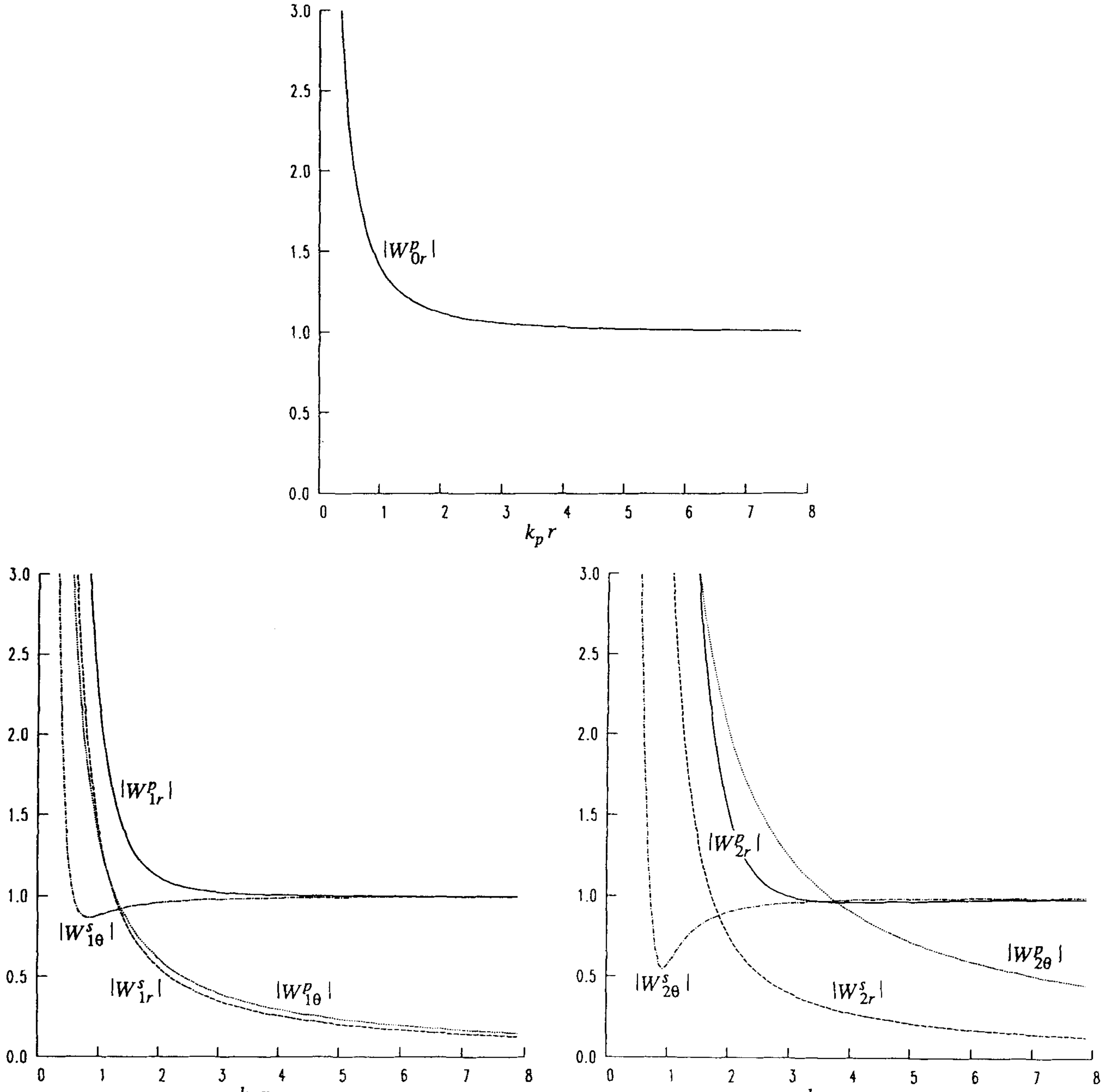

Figure 1. Moduli of the W functions which control the distance dependence of the scattered fields in the low-frequency approximation.

This result represents Rayleigh scattering from an obstacle having an arbitrary contrast in material properties. In the case where the contrast is small and the conditions of eq. (3) are satisfied, then eq. (22) reduces to (6) and we have the combined approximations of low frequency, far field and low contrast. Thus the progression of solutions in eqs (13), (19), (22) and (6) shows the effects of the Rayleigh and Born approximations.

The Mie scattering solution for a homogeneous sphere in eq. (11) can be easily generalized to a sphere of arbitrary contrast to obtain

$$\mathbf{U}_p = A\left\{-\frac{1}{2}\frac{\frac{3}{2}(\lambda_1-\lambda_2)+\mu_1-\mu_2}{\frac{1}{2}(\frac{3}{2}\lambda_1+\mu_1)+\mu_2}+\left(\frac{\rho_1}{\rho_2}-1\right)\cos\theta+\frac{2}{3}\left(\frac{\mu_1}{\mu_2}-1\right)\frac{\gamma^2}{D}(1-3\cos^2\theta)\right\}\frac{j_1(q_1)}{q_1}\hat{\mathbf{r}} \tag{23a}$$

$$\mathbf{U}_s = B\left\{-\left(\frac{\rho_1}{\rho_2}-1\right)\sin\theta+\left(\frac{\mu_1}{\mu_2}-1\right)\frac{\gamma}{D}\sin 2\theta\right\}\frac{j_1(q_2)}{q_2}\hat{\boldsymbol{\theta}}. \tag{23b}$$

In order to compare the various approximations discussed above, the normalized cross-sections of eq. (15) are plotted as a function of k_pR in Fig. 3. Such results are shown for two different cases, a low-velocity inclusion on the top and a high-velocity

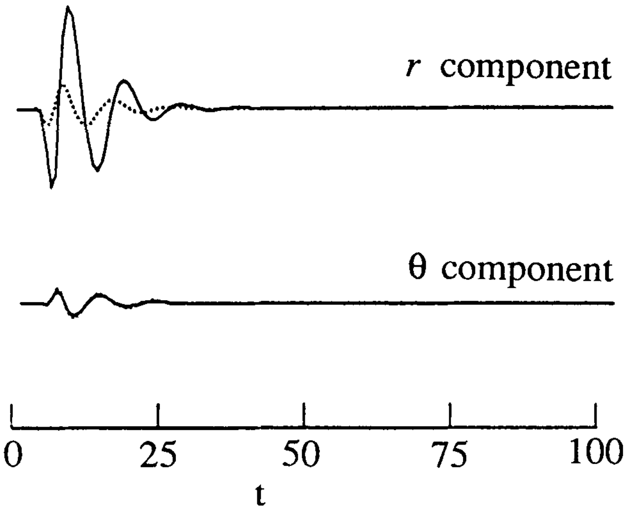

Figure 2. Synthetic seismograms that show the effects of near-field terms in the scattered fields. A plane P wave is incident upon a high-velocity sphere for which $V_{p_1}/V_{p_2} = V_{s_1}/V_{s_2} = 1.25$ and $\rho_1/\rho_2 = 1.10$. The dominant angular frequency of the input pulse is $\omega = 0.2V_p/R$, where R is the radius of the sphere. The seismograms are calculated at a radial distance $r = 6R$ and an azimuth $\theta = 45°$. The units of the time t are R/V_p. The solid line is the complete solution, whereas the dotted line includes only the far-field parts of the solution.

inclusion on the bottom. The contrast in the velocities and densities is about 20 per cent. The four solutions shown in this figure are the exact of eq. (13), the Born–Rayleigh approximation of eq. (6), the arbitrary contrast Rayleigh of eq. (22), and the arbitrary contrast Mie of eq. (23). Note that the near-field terms do not contribute to the scattering cross-sections. In order to calculate scattering cross-sections from the solution in eq. (23) it was necessary to convert this solution to the form of eq. (13) using the orthogonal properties of the spherical vectors in eq. (14), and then substitute the obtained coefficients a_l and b_l into eq. (15). It should be pointed out that scattering cross-sections for the case of Rayleigh scattering from a spherical inclusion of arbitrary contrast were also obtained by Ying & Truell (1956) using potential functions.

The results shown in Fig. 3 help define the frequency ranges over which the various approximations are valid. First note that the Born–Rayleigh approximation is the least accurate of those shown in this figure and that the sign of the error is different for low-velocity and high-velocity inclusions. For the case of the low-velocity inclusion, this approximation falls below the exact solution at low frequencies, and the error reaches appreciable values in the range around $k_pR = 0.4$, whereas in the case of the high-velocity inclusion the approximate solution falls above the exact solution and the error exceeds 100 per cent for $k_pR > 0.3$. In contrast to this, the arbitrary contrast Rayleigh approximation behaves about the same for the low-velocity and high-velocity inclusions and remains reasonably accurate for $k_pR < 0.5$. A result which is very clear in this figure is that by far the best approximation to the exact solution is provided by the arbitrary contrast Mie solution. This approximation is reasonably valid for $k_pR < 6$ for the low-velocity inclusion and for $k_pR < 4$ for the high-velocity inclusion, which is an order of magnitude broader range than for the other approximations. Of course, these ranges of validity will vary somewhat with the values of the material properties which are used, but our calculations indicate that the results shown in Fig. 3 display the primary features present in the general case.

5 LOW-CONTRAST APPROXIMATION

Another type of approximate solution which can be derived from the exact solution of Section 3 is one which assumes a small contrast in material properties between the inclusion and surrounding media, but places fewer restrictions upon the applicable frequency range than does the Rayleigh approximation. For the case in eq. (3) of small perturbations in the elastic parameters of the inclusion, the coefficients a_l and b_l of eq. (13) (the original expressions can be found in Appendix B of Korneev & Johnson 1993) can be reduced to the following expressions

$$a_l = i\xi^3\left\{\frac{1}{2}\frac{\delta\lambda + 2\delta\mu}{\lambda + 2\mu}[j_l^2(\xi) - j_{l+1}(\xi)j_{l-1}(\xi)] + \frac{\delta\mu}{\lambda + 2\mu}\frac{2}{\xi^2}\left[l(l-1)\frac{j_l(\xi)}{\xi}(j_{l-1}(\xi) - j_{l+1}(\xi)) - 2j_{l+1}^2(\xi)\right]\right.$$
$$\left.-\frac{1}{2}\frac{\delta\rho}{\rho}\left[j_l^2(\xi) + j_{l+1}^2(\xi) - (2l+3)\frac{j_l(\xi)}{\xi}j_{l+1}(\xi) + 2l\frac{j_l^2(\xi)}{\xi^2}\right]\right\} \tag{24a}$$

$$b_l = i\eta^3\left\{\frac{\delta\mu}{\lambda + 2\mu}\frac{2}{\xi^2}\left[j_{l+1}(\eta)\left((l-1)\frac{j_l(\xi)}{\xi} - j_{l+1}(\xi)\right) - (l-1)\frac{j_l(\eta)}{\eta}j_{l-1}(\xi)\right] + \frac{\delta\rho}{\rho}\frac{j_l(\eta)}{\eta}\frac{j_l(\xi)}{\xi}\right\}. \tag{24b}$$

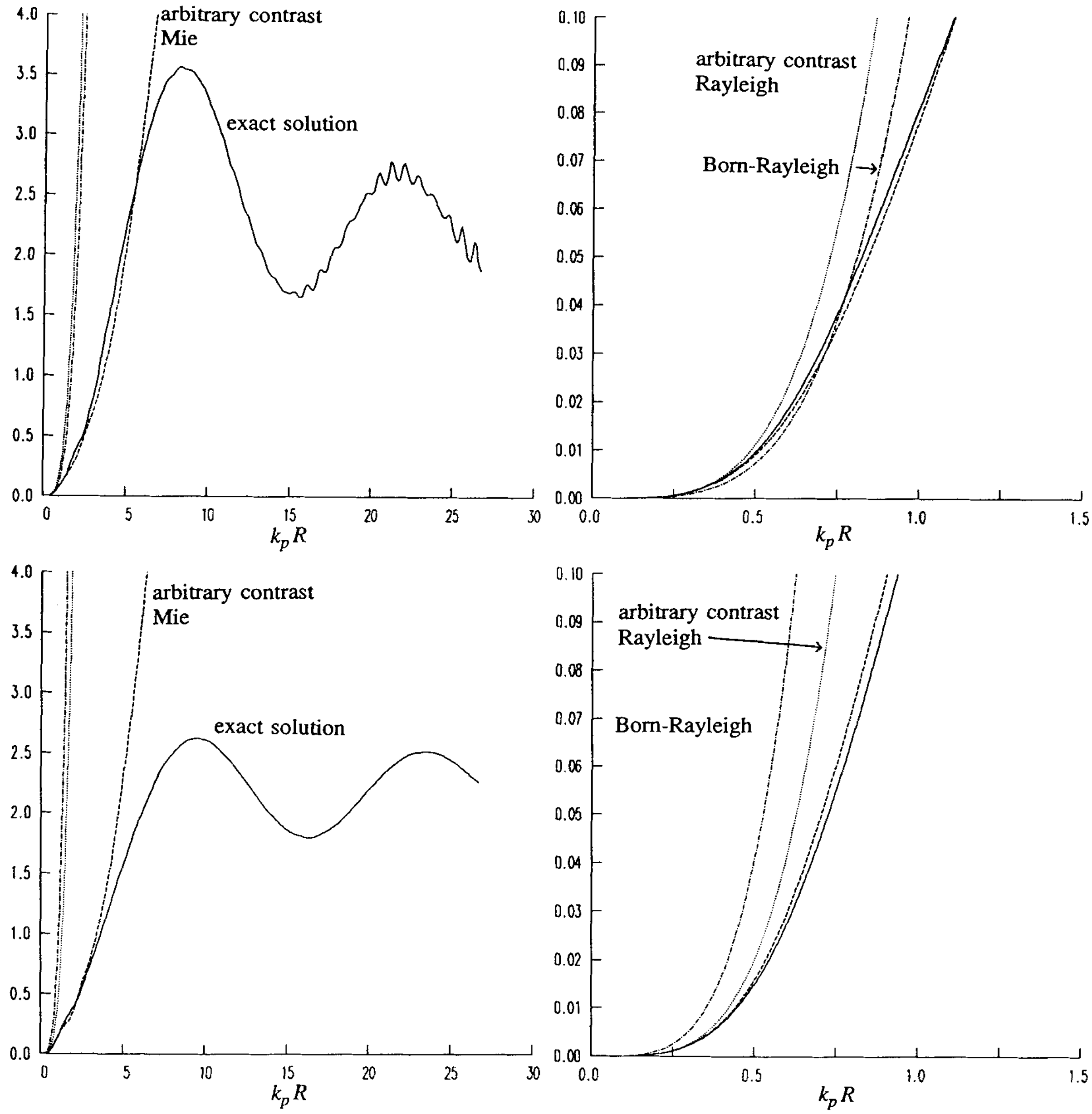

Figure 3. Normalized scattering cross-sections as a function of frequency. The upper two panels are for a low-velocity inclusion with $V_{p_1}/V_{p_2} = V_{s_1}/V_{s_2} = 0.8$ and $\rho_1/\rho_2 = 0.9$, while the lower panels are for a high-velocity inclusion with $V_{p_1}/V_{p_2} = V_{s_1}/V_{s_2} = 1.3$ and $\rho_1/\rho_2 = 1.2$. The panels on the right are expanded versions of those on the left for small values of the arguments.

These solutions are not completely general in frequency, because the manipulations of the Bessel functions that were used in obtaining them are only strictly valid when we have

$$\xi_1 - \xi_2 \approx k_p R \frac{1}{2}\left(\frac{\delta\lambda + 2\delta\mu}{\lambda + 2\mu} - \frac{\delta\rho}{\rho}\right) < \frac{\pi}{10}, \qquad \eta_1 - \eta_2 \approx k_s R \frac{1}{2}\left(\frac{\mu}{\mu} - \frac{\delta\rho}{\rho}\right) < \frac{\pi}{10}. \tag{25}$$

This restriction places an upper limit upon the valid frequency range for eq. (24), with this limit increasing as the contrast in material properties becomes smaller and smaller. Below we will show that this restriction is significant for the a_l coefficients but not for the b_l coefficients.

Given that the low-contrast solution of eq. (24) is most appropriate for low frequencies that satisfy the restriction of eq. (25), we can proceed differently to obtain solutions that are more appropriate for the higher frequencies. Here we follow the method described by Van der Hulst (1957) for the scattering of light from large low-contrast spheres. The basic procedure is to substitute Debye asymptotic expansions for the Bessel functions into the exact analytical expressions. Starting with the exact analytical expressions for the coefficients of eq. (13), the low-contrast assumption is made and then it is possible to obtain the following approximate expression for the coefficients of the scattered P wave.

$$a_l \approx -\frac{j_{l+1}(\xi_1)j_l(\xi_2) - \kappa j_l(\xi_1)j_{l+1}(\xi_2)}{j_{l+1}(\xi_1)h_l(\xi_2) - \kappa j_l(\xi_1)h_{l+1}(\xi_2)} \tag{26}$$

where

$$\kappa = \frac{\rho_1 V_{p_1}}{\rho_2 V_{p_2}}.$$

Then we write eq. (26) in the form

$$a_l = -\frac{\tan(\alpha_l)}{\tan(\alpha_l) - i} = -\frac{1}{2}(1 - e^{-2i\alpha_l}) \tag{27}$$

where

$$\tan(\alpha_l) = -\frac{j_{l+1}(\xi_1)j_l(\xi_2) - \kappa j_l(\xi_1)j_{l+1}(\xi_2)}{j_{l+1}(\xi_1)n_l(\xi_2) - \kappa j_l(\xi_1)n_{l+1}(\xi_2)}$$

and the $n_l(\xi)$ are spherical Neuman functions. Because we are looking for solutions valid at high frequencies, we introduce the Debye asymptotic expansions

$$j_l(\xi) = \frac{\cos\left(\xi f - \frac{\pi}{4}\right)}{\xi\sqrt{\tau}}$$

$$n_l(\xi) = -\frac{\sin\left(\xi f - \frac{\pi}{4}\right)}{\xi\sqrt{\tau}}$$

where

$$f = \sin\tau - \tau\cos\tau, \quad \text{and} \quad \cos\tau = \frac{l + \frac{1}{2}}{\xi}.$$

These approximations are valid for $l + \frac{1}{2} < \xi$. Now eq. (27) can be reduced to

$$a_l = -\frac{1}{2}\left(1 - e^{2i(\xi_2 f_2 - \xi_1 f_1)}\frac{1 - ike^{2i\xi_1 f_1}}{1 + ike^{-2i\xi_1 f_1}}\right) \tag{28}$$

where

$$k = \frac{\kappa - 1}{\kappa + 1}.$$

If the low-contrast conditions of eq. (3) are strongly satisfied, eq. (28) can be further simplified to yield

$$a_l = -\tfrac{1}{2}(1 - e^{-ia}) \tag{29}$$

where

$$a = 2\left(1 - \frac{V_{p_1}}{V_{p_2}}\right)\xi. \tag{30}$$

This is identical to the solution that is obtained in optics. Substituting the a_l of eq. (29) into the optical theorem of eq. (16) results in a simple formula for the normalized scattering cross-section (Morochnik 1983).

$$\sigma_N \approx \sigma_N^{(p)} \approx 2 - \frac{4}{a}\sin a + \frac{4}{a^2}(1 - \cos a). \tag{31}$$

An earlier derivation of eq. (31) can be found in Van der Hulst (1957), where it is shown that this result can be explained by interference of the incident and refracted waves propagating in the forward direction. The parameter a is just the phase difference between these two waves in the far field.

Two different formulae have been developed above for the coefficients of the scattered P waves in the low-contrast case. At frequencies low enough so that (25) is satisfied, eq. (24a) should be used. At higher frequencies eq. (28) should be used, and when the low-contrast assumption is strongly satisfied this can be replaced by eq. (29). The high-frequency solution is valid so long as $\xi \leq l + \frac{1}{2}$. The relationship between these different approximate solutions for the scattered P wave is illustrated in

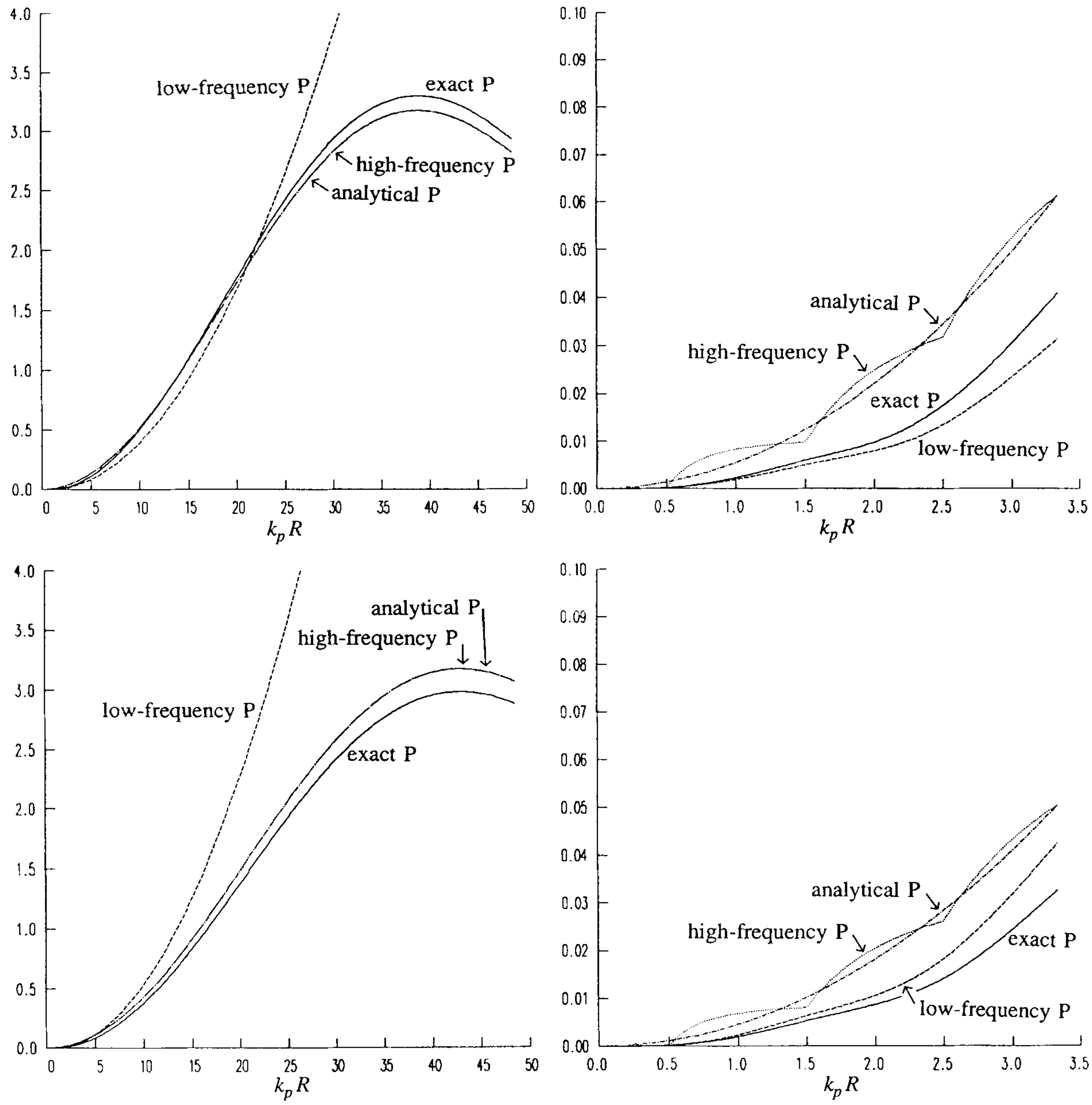

Figure 4. Normalized scattering cross-sections as a function of frequency for the scattered P field in the low-contrast case. The upper two figures are for a low-velocity inclusion with $V_{p_1}/V_{p_2} = V_{s_1}/V_{s_2} = \rho_1/\rho_2 = 0.95$, while the lower figures are for a high-velocity inclusion with $V_{p_1}/V_{p_2} = V_{s_1}/V_{s_2} = \rho_1/\rho_2 = 1.05$. The panels on the right are expanded versions of those on the left for small values of the arguments.

Fig. 4 for two different cases, a low-velocity inclusion and a high-velocity inclusion. In both cases the contrast in velocities and densities is about 5 per cent. This figure shows the scattering cross-section of the exact solution for the scattered P field of eq. (13) and for two approximate solutions, the low-frequency P field of eq. (24) and the high-frequency P field of eq. (28). Also shown is the scattering cross-section which is calculated using the analytical expression of eq. (31). At low frequencies the approximate solution of eq. (24a) agrees best with the exact solution for the scattered P field, with the error growing to about 30 per cent by the time that the condition of eq. (25) is exceeded ($k_pR \approx 3$). The high-frequency approximate solution in eq. (28) as well as eq. (31) both systematically over estimate the exact solution in this range. At higher frequencies the situation is reversed. The low-frequency approximate solution of eq. (24a) tracks the exact solution reasonably well up to about $k_pR \approx 5$ and then is completely wrong at higher frequencies. The high-frequency approximate solution of eq. (28) and eq. (31) agree quite well with the exact solution for $k_pR \geq 5$, showing the same oscillatory behaviour at a slightly reduced amplitude for the low-velocity inclusion and at a slightly increased amplitude for the high-velocity inclusion. In this range these two approximate results are so close to each other that they appear as one line on the graph. This demonstrates that the very simple analytical expression of eq. (31) provides an excellent approximation to the scattering cross-section for the high-frequency low-contrast case.

For the scattered S waves in the low-contrast approximation we return to eq. (24b) for the b_l coeficients. In this case the condition of eq. (25) does not restrict the use of eq. (24b) because the higher order b_l coefficients decrease sufficiently rapidly with increasing frequency. At high frequencies the S part of the scattering cross-section, $\sigma_N^{(s)}$, oscillates slightly about a constant level. Substituting eq. (24b) into eq. (15) for $\sigma_N^{(s)}$ and numerically evaluating the infinite sum of the products of Bessel functions, we obtain the high-frequency asymptotic estimate

$$\begin{aligned}\sigma_N^{(s)} &= 4\sum_{l\geq 0}^{\infty} l(l+1)(2l+1)\gamma\left|\frac{b_l}{\eta}\right|^2 \\ &\approx 4.2\gamma^4\frac{\delta\mu^2}{\mu^2} - 6.0\gamma^{\frac{13}{4}}\frac{V_{s_1}^2}{V_{s_2}^2}\frac{\delta\mu}{\mu}\frac{\delta\rho}{\rho} + 1.8\gamma^{\frac{5}{4}}\frac{\delta\rho^2}{\rho^2}.\end{aligned} \tag{32}$$

Thus we see that in the limit of large frequency, the scattering cross section of the S waves reduces to a constant independent of frequency.

An example of the various solutions for the normalized scattering cross-sections for the S field is shown in Fig. 5. It is clear that the low-contrast solution calculated from eq. (24b) is a good approximation to the exact solution for both cases of a

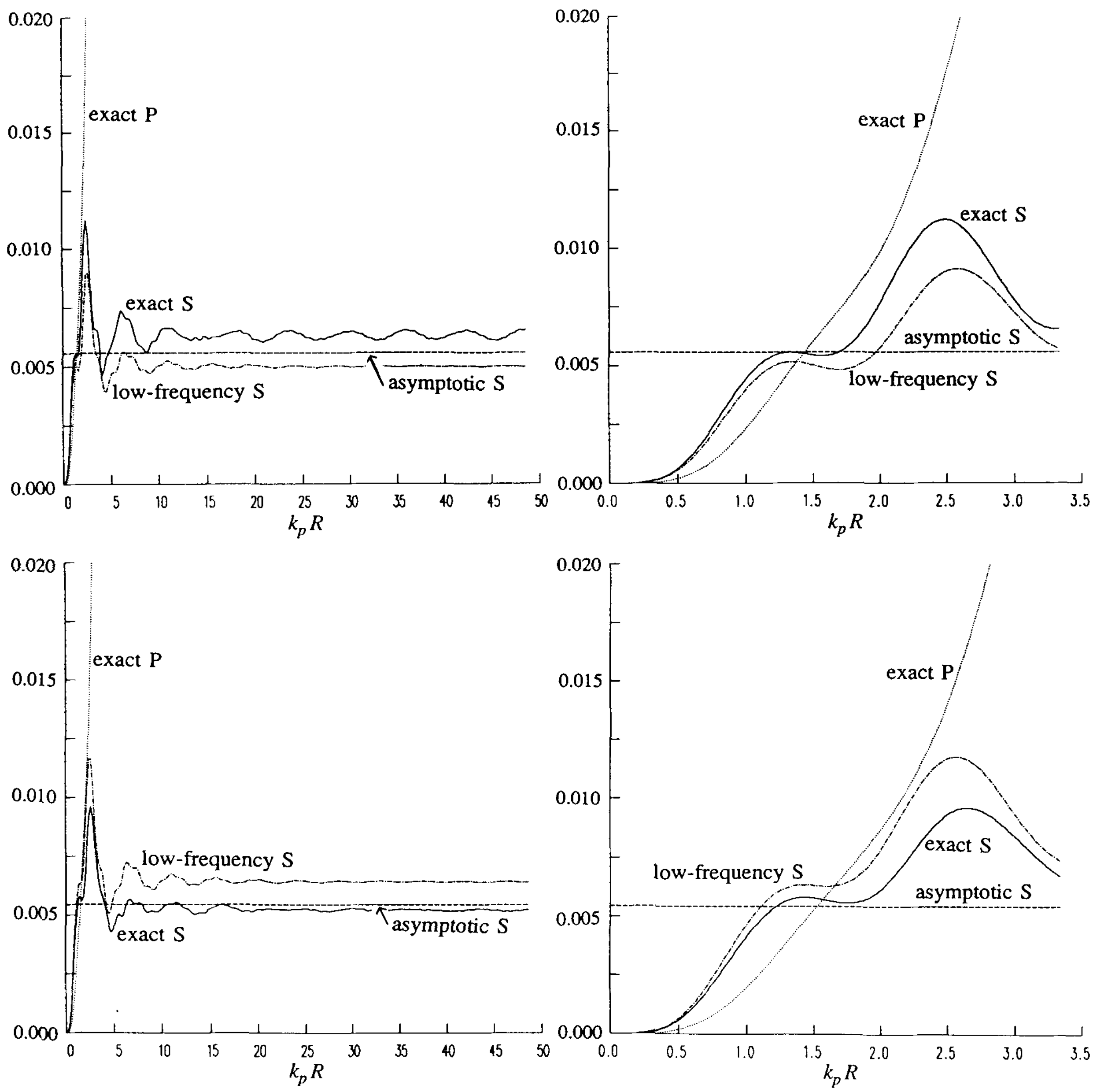

Figure 5. Similar to Fig. 4 for the scattered S field. Also shown for comparison is the exact P field from Fig. 4.

low-velocity inclusion and a high-velocity inclusion. The agreement is extremely good for $k_pR < 1$, but even at higher frequencies the approximate result tracks the main features of the exact result and never differs from it by more than about 25 per cent. Similar to the scattered P field, this approximate solution underestimates the exact solution in the case of a low-velocity inclusion and over estimates it in the case of a high-velocity inclusion. Also shown on this plot is the high-frequency asymptotic approximation of eq. (32). While this is obviously not an appropriate approximation at the very low frequencies, it provides a simple but fairly accurate result at higher frequencies. It is worth noting that the examples shown in Figs 4 and 5 actually represent a severe test for the low-contrast approximations. While the contrasts in velocites and densities are only 5 per cent in these examples, the contrasts in elastic constants are about 15 per cent.

Also shown in Fig. 5 for the purposes of comparison is the exact solution for the normalized scattering cross section of the P field. The scattered P field is clearly much larger than the scattered S field for high frequencies, but for $k_pR < 1$ the situation can be reversed, with the scattered S field considerably larger than the scattered P field. To a certain degree this type of behaviour is a function of the contrasts in material properties of the inclusion, but there is generally a range of frequencies where more energy is scattered into the S field than into the P field. This observation could have implications for the generation of seismic coda.

6 CONCLUSIONS

There are two basic lessons to be learned from this study. First, considerable care must be taken in using various approximate solutions for the seismic scattering problem because these solutions are valid only over a limited range of conditions. Second, standard approximations that are typically made in seismology and associated with the names of Born, Rayleigh and Mie, can be considerably improved by making a few modifications in the formulae or by using some of the alternative formulae developed in this study. Because of the need to make comparisons with exact solutions, this study has concentrated on the case of P waves scattered from a spherical inclusion. However, the results are more general than this and should be applicable to scattering from a more extended class of objects with simple and smooth boundaries.

The Born–Rayleigh approximation is commonly made in seismology for the case of low-contrast scatterers and wavelengths large compared to the dimensions of the scatterer. However, because of the effect of near-field terms in the scattering solution, this approximation is only valid at distances which are removed several wavelengths from the site of the scattering. Thus care must be taken in using this type of an approximation to explain scattering in the vicinity of seismographic stations.

Both the usual Rayleigh approximation of eq. (6) and the Mie approximation of eq. (10) are limited to low frequencies and low contrasts in material properties. The low-contrast limitation can be considerably expanded by using solutions developed as a low-frequency approximation for an inclusion of arbitrary contrast. Thus, by substituting eq. (22) for the Rayleigh formula of eq. (6) and by substituting eq. (23) for the Mie formula of eq. (11), the range of validity of these solutions can be extended to higher frequencies. In particular, as shown in Fig. 3, the arbitrary contrast Mie solution is valid over a frequency range that is an order of magnitude greater than for the other approximate solutions.

In situations where the contrast in material properties is actually small, approximate solutions have been developed that are valid over essentially the entire frequency range. In the case of an incident P wave two different results must be used for the scattered P field, one for the low frequencies and one for the high frequencies. However, a single result can be used for the scattered S field over the entire frequency range. For situations where the scattering cross-section is needed, an analytical result based on the optical theorem provides a simple but good approximation for the higher frequencies. Finally, these results illustrate some of the important differences between acoustic and elastic scattering, as there are frequencies where considerably more energy is scattered into S waves than into P waves.

ACKNOWLEDGMENTS

This research was supported by Phillips Laboratory under Contract F19628-90-K-0055 and also by the US Department of Energy under Contract DE-AC03-76SF00098.

REFERENCES

Aki, K. & Chouet , B., 1975. Origin of coda-waves: attenuation and scattering effects, *J. geophys. Res.*, **80,** 3322–3342.

Chernov, L. A., 1960. *Wave Propagation in a Random Medium,* English translation, Dover, New York.

Hudson, J. A. & Heritage, J. R., 1981. The use of the Born approximation in the seismic scattering problem, *Geophys. J. R. astr. Soc.*, **66,** 221–240.

Korneev, V. A. & Johnson, L. R., 1993. Scattering of elastic waves by a spherical inclusion—I. Theory and numerical results, *Geophys. J. Int.*, **115,** 230–250, (this issue).

Morochnik, V. S., 1983. Scattering of compressional elastic waves by a low-contrast spherical inclusion, *Iz. Acad. Nauk USSR, Fizika Zemli,* **7,** 65–72 (in Russian).

Sato, H., 1984. Attenuation and envelope formation of three-component seismograms of small local earthquakes in randomly inhomogeneous lithosphere, *J. geophys. Res.,* **89,** 1221–1241.

Van der Hulst, H. C., 1957. *Light Scattering by Small Particles,* Wiley, New York.

Wu, R. & Aki, K., 1985a. Scattering characteristics of elastic waves by an elastic heterogeneity, *Geophysics,* **50,** 582–595.

Wu, R. & Aki, K., 1985b. Elastic wave scattering by a random medium and the small-scale inhomogeneities in the lithosphere, *J. geophys. Res.,* **90,** 10 261–10 273.

Ying, C. F. & Truell, R., 1956. Scattering of a plane longitudinal wave by a spherical obstacle in an isotropically elastic solid, *J. appl. Physics,* **27,** 1086–1097.